

Properties of the NiAs-Type Phase $\text{Ni}_{1+m}\text{Sn}_{1-x}\text{P}_x$

Sigrid Furuseth* and Helmer Fjellvåg

Department of Chemistry, University of Oslo, N-0315 Oslo 3, Norway

Furuseth, S. and Fjellvåg, H., 1994. Properties of the NiAs-Type Phase $\text{Ni}_{1+m}\text{Sn}_{1-x}\text{P}_x$. – Acta Chem. Scand. 48: 134–138 © Acta Chemica Scandinavica 1994.

The conditions for the existence of an $\text{Ni}_{1+m}\text{Sn}_{1-x}\text{P}_x$ solid solution phase with a partly filled NiAs-type structure are described. The phase has a large homogeneity region at high temperatures which includes Ni_3Sn_2 . At room temperature, the phase exists only for a small composition range (in x, m). Metastable one-phase samples were obtained on quenching. Single-crystal X-ray and powder neutron diffraction data provide weak indications for deviations from the ideal structure. A tendency towards formation of NiP_3Sn_2 clusters at the trigonal bipyramidal sites is proposed. Thermal expansion data are presented for the quenched, metastable NiAs-type phase, and transformations into stable products are described. The phase exhibits Pauli paramagnetism.

Most NiX and NiY phases, $X = \text{Si, Ge, Sn}$ and Pb and $Y = \text{P, As, Sb}$ and Bi , crystallize with the NiAs-type structure or the closely related MnP-type structure.^{1–7} NiSn and NiP deviate from this trend by adopting their own structure types.^{8,9} A characteristic feature of binary NiAs- and MnP-type phases is their tendency to extend into pseudobinary solid solution phases. Only a few reports concern solid solution systems involving both main-group 14 and 15 non-metal elements.¹⁰ An earlier study of the Ni–Sn–P ternary system revealed the existence of a stoichiometric Ni_2SnP compound.¹¹ Its orthorhombic structure shows a resemblance to the MnP type, but instead of randomly distributed non-metal atoms, there is a complete ordering of Sn and P atoms. During the study of Ni_2SnP , clear indications of the existence of a ternary phase in the Ni–Sn–P system of the NiAs-type were found. The present communication reports the preparation, homogeneity region and structural and physical properties for this phase, whose maximum extensions are described by the general formula $\text{Ni}_{1+m}\text{Sn}_{1-x}\text{P}_x$ ($0.00 \leq m \leq 0.65, 0.00 \leq x \leq 0.32$).

Experimental

Preparation. Samples of $\text{Ni}_{1+m}\text{Sn}_{1-x}\text{P}_x$ were prepared by heating weighed amounts of the elements (Ni, turnings from rods, 99.99%; Johnson, Matthey Laboratories Ltd.; Sn, granules, 99.9% Fluka AG; P, lumps, 99.999%, Koch-Light Laboratories, Ltd.) in evacuated, sealed silica glass ampoules. After a first heating at 1075 K for 1 week,

the samples were cooled to room temperature, crushed and subjected to one similar heat treatment before finally being quenched in ice-water from temperatures between 975 and 1175 K. Additional samples (generally two- or multi-phased) were obtained by slow cooling from 1075 K to room temperature during 5 days.

Single crystals of metal-rich $\text{Ni}_{1+m}\text{Sn}_{1-x}\text{P}_x$ were grown in tin melts (molar ratio Ni:Sn:P \approx 4:40:1) inside evacuated silica glass tubes. The temperature was lowered from 1375 to 1075 K over 2 days, and the samples were subsequently quenched in ice-water. The Sn surplus was dissolved in hydrochloric acid, and needle-formed crystals with metallic lustre and size up to $0.5 \times 0.1 \times 0.1$ mm were obtained.

Characterization. All samples were characterized by powder X-ray diffraction (PXD) using Guinier–Hägg cameras, $\text{CuK}\alpha_1$ radiation and Si as internal standard. The homogeneity region was deduced on the basis of the disappearing phase principle and by comparison of unit-cell dimensions. The reflections in the powder diffraction pattern and their relative intensities immediately indicated a crystal structure basically of the NiAs type for the $\text{Ni}_{1+m}\text{Sn}_{1-x}\text{P}_x$ solid solution phase.

Powder neutron diffraction (PND) data were collected for $\text{Ni}_{1.17}\text{Sn}_{0.69}\text{P}_{0.31}$ at 295 K with the OPUS III two-axis diffractometer at the JEEP II reactor, Kjeller, using monochromatized neutrons of wavelength 187.7 pm. Data were collected in steps of 0.05° between $2\theta = 10$ and 90° . Profile refinements were carried out using the Hewat version¹² of the Rietveld program. The scattering lengths $b_{\text{Ni}} = 10.3$, $b_{\text{Sn}} = 6.228$ and $b_{\text{P}} = 5.13$ fm were adopted.

* To whom correspondence should be addressed.

High-temperature PXD data were collected between 300 and 1200 K using an Enraf-Nonius Guinier–Simon camera. The temperature change was synchronized with the movement of the film cassette. At high temperatures, say 1200 K, the Ni–Sn–P samples tended to become oxidized in the quartz capillaries with partial formation of SnO_2 and NiO. The problem was circumvented by using double, sealed capillaries.

Magnetic susceptibility data were collected between 4 and 300 K using a SQUID system (MPMS, Quantum Design) and a magnetic field of 500 G. DSC measurements were carried out between 100 and 900 K with a Mettler TA 3000 system, and DTA measurements between 300 and 1400 K with a Netzsch 404EP thermo-analyzer.

X-Ray intensity data collection. Single-crystal X-ray diffraction intensity data were collected for $\text{Ni}_{1.16}\text{Sn}_{0.68}\text{P}_{0.32}$ at 295 K with a Syntex P1 auto-diffractometer in the θ – 2θ scan mode using $\text{MoK}\alpha$ radiation. No significant time fluctuations were observed for three standard reflections. For scattering angles up to $2\theta = 90^\circ$ a total of 255 reflections were measured, of which 109 unique reflections with $I \geq 3\sigma(I)$. The observed intensities were in full accordance with the adopted space group $P6_3/mmc$. Corrections for Lorentz and polarization effects, absorption and isotropic extinction as well as the least-squares refinements, minimizing $\sum w(|F_o| - |F_c|)^2$ with $w = 1/\sigma^2(F_o)$, were performed using the GX program system.¹³

Results and discussion

Solid solubility and phase diagram. In the binary Ni–Sn and Ni–P systems, only the high-temperature modification of Ni_3Sn_2 takes the NiAs-type structure (or more correctly, a partly filled variant).^{14,15} On the other hand, $\text{Ni}_{7\pm x}\text{Sn}_8$, $\text{Ni}_{3+x}\text{Sn}_4$, NiSn and NiP all show more-or-less pronounced structural relationships to the NiAs-type structure.^{11,16} Within the ternary Ni–Sn–P system, it thus seems reasonable to search for NiAs-type related phases for metal/non-metal ratios around 1 and 1.5.

Homogeneous, single-phase samples of $\text{Ni}_{1+m}\text{Sn}_{1-x}\text{P}_x$ with the NiAs-type structure were obtained by quenching from elevated temperatures for a fairly large interval in m and x (Figs. 1a and 1b). For a restricted composition range, single-phase samples were also obtained by slow cooling (Fig. 1c). Otherwise, slow cooling resulted in a phase separation (e.g. into $\text{Ni}_{7\pm x}\text{Sn}_8$ and Ni_2P for $m \leq 0.2$).

The homogeneity region is strongly temperature dependent. Its extension is shown schematically for samples quenched from 1125 and 975 K, as well as for samples slowly cooled to room temperature, in Fig. 1. At the lower temperatures, two separate regions with substantial Sn(P) substitution exist, one centered around $m = 0.50$ and another around $m = 0.10$. At 1125 K the two regions merge at low P contents (x). Note that no stoichiometric 1:1 NiAs-type phase exists.

The variation of the unit-cell dimensions (at 295 K) is shown in Fig. 2 for samples quenched from 1125 K

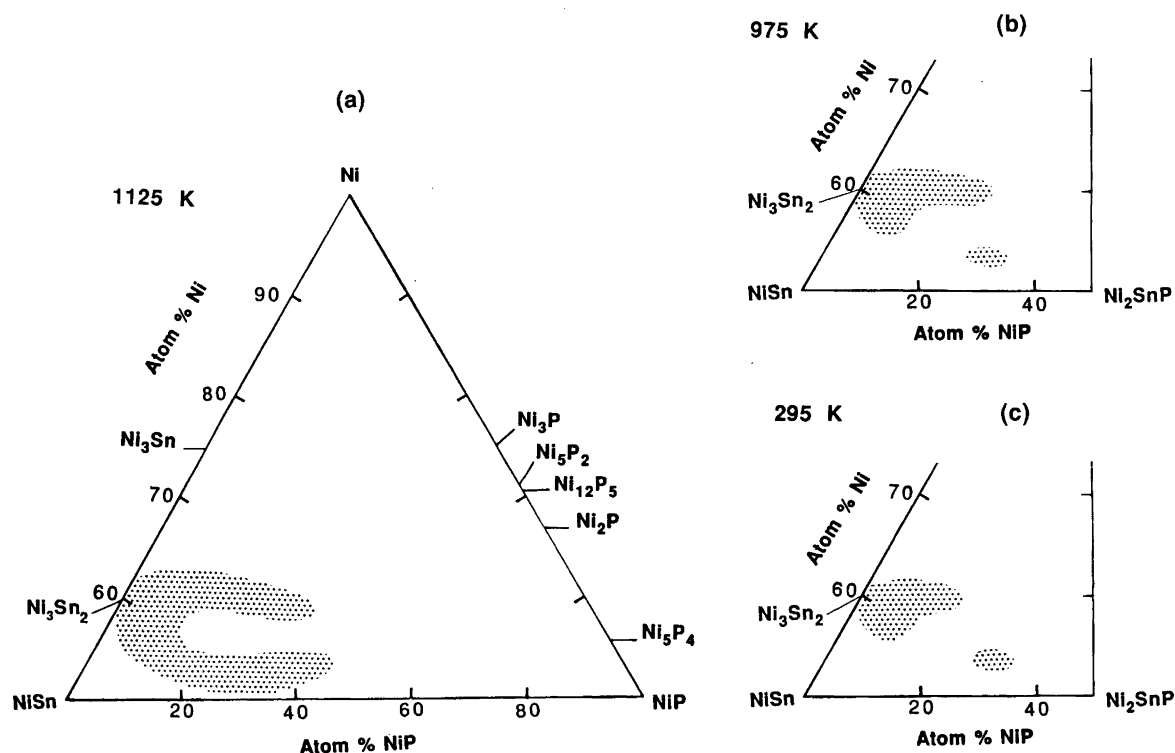


Fig. 1. Section of the Ni–Sn–P phase diagram at (a) 1125, (b) 975 and (c) 295 K (judged from slowly cooled samples).

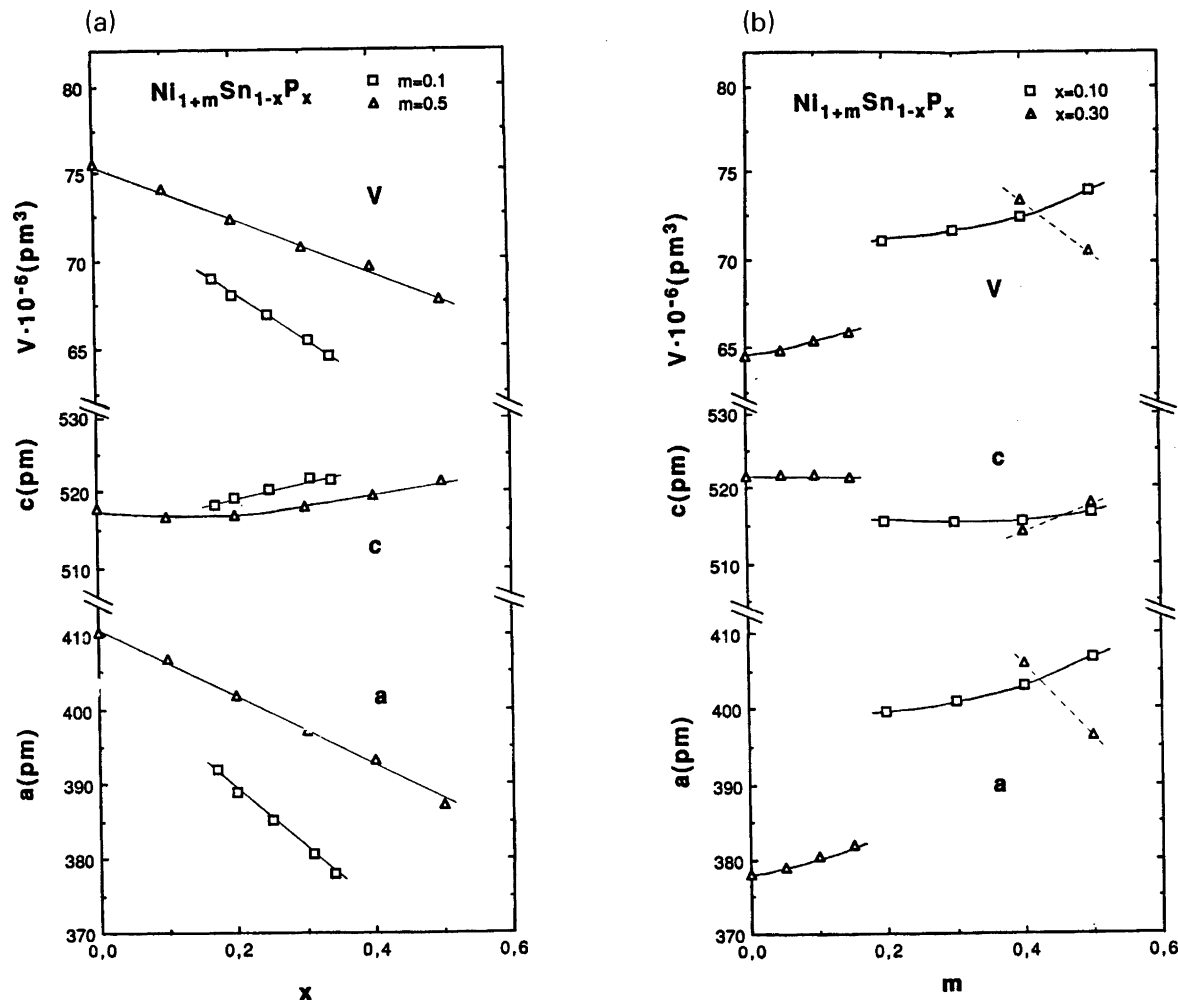


Fig. 2. Variation of unit-cell dimensions versus composition (m , x) for samples of $\text{Ni}_{1+m}\text{Sn}_{1-x}\text{P}_x$ quenched from 1125 K; (a) for $m=0.10$ and 0.50 (b) for $x=0.10$ and 0.30 . Calculated standard deviations do not exceed the size of the symbols.

(cf. also the phase diagram data in Fig. 1). As expected, the volume decreases upon increasing the P content (Fig. 2a; m constant) and upon decreasing the Ni content (Fig. 2b; x constant). The variation of the unit-cell dimensions in Fig. 2b for $\text{Ni}_{1+m}\text{Sn}_{0.70}\text{P}_{0.30}$ reflects the phase diagram situation (Fig. 1), with the existence of two separate NiAs-type phases. (The nominal $m=0.45$ sample contains additional Ni_{12}P_5 , and hence the unit-cell data cannot be taken as indicators for the real behaviour of $\text{Ni}_{1+m}\text{Sn}_{0.70}\text{P}_{0.30}$.) For all samples, the c -axis remains fairly constant throughout the entire homogeneity range, whereas a varies significantly. Thus the c/a axial ratio varies between 1.27 and 1.38, which are typical values for NiAs-type phases of the 'heavier' 3d-elements.

For slowly cooled samples of $\text{Ni}_{1.5}\text{Sn}_{1-x}\text{P}_x$, an orthorhombic superstructure ($a_o = a_h + 2b_h$; $b_o = c_h$; $c_o = 2a_h$; $V_o = 4V_h$) appears, with ordering between 'interstitial' Ni atoms and vacancies.¹⁶ For $x=0.00$ and 0.10 , the order-disorder transition occurs rather abruptly at $T_d = 750 \pm 10$ K.

Atomic arrangement. The single-crystal X-ray diffraction data confirmed the NiAs-type structure with the additional Ni(2) atoms in trigonal bipyramidal holes (2c site) between close-packed (2d site) non-metal atoms (final $R = 0.063$, $R_w = 0.061$). In the refinements the Sn and P atoms were assumed to be randomly distributed over the non-metal sublattice. For the crystal, $a = 377.9(1)$ and $c = 521.7(1)$ pm. The refined Sn (and P) content ($x = 0.316 \pm 0.028$) corresponds well to that deduced on the basis of unit-cell data (cf. Fig. 2). The occupancy of Ni(2) in the 2c sites is refined to 0.16 ± 0.02 . The values for the temperature factors are $u_{\text{Ni}(1),11} = 0.071(4)$, $u_{\text{Ni}(1),33} = 0.023(2)$, $u_{\text{Ni}(1),12} = 0.049(7)$, $u_{\text{Ni}(2),\text{iso}} = 0.063(13)$, $u_{\text{Sn},11} = 0.017(1)$, $u_{\text{Sn},33} = 0.029(2)$, $u_{\text{Sn},12} = 0.010(2)$, $u_{\text{P},\text{iso}} = 0.022(11)$. The temperature factors are rather large for Ni(1) and Ni(2), and may indicate (static) deviations from the ideal structure, see below.

The main features of the PND patterns are consistent with an NiAs-type structure; however, some inconsistencies are evident. Firstly, a pronounced and diffuse intensity contribution to the background exists around (102).

Secondly, the overall fit is not satisfactory ($R_p \approx 20$, $R_{\text{expected}} \approx 8$), which contrasts the single-crystal X-ray diffraction study that gave fairly acceptable fits, although not as good as otherwise expected for a crystal of good quality. A main difference between the two diffraction studies is that Ni is by far the best scatterer with respect to neutrons, whereas Sn has the highest scattering power with respect to X-rays. It is thus tempting to suggest that the Ni atoms may be shifted out of their ideal positions.

The Ni(2) atoms in the trigonal bipyramidal holes have five non-metal neighbours at distances $a/\sqrt{3} \approx 220$ pm ($3 \times$) and $c/2 \approx 260$ pm ($2 \times$). The longer distances are of the order of normal Ni–Sn distances (cf. e.g. $\text{Ni}_{7 \pm x}\text{Sn}_8$,^{8,17} $\text{Ni}_{3+x}\text{Sn}_4$,^{17,18} NiSn ,⁸ $\text{Ni}_2\text{SnP}^{11}$), whereas the shorter ones are close to normal Ni–P separations (cf. e.g. NiP ,⁹ NiP_2 ,⁹ $\text{Ni}_2\text{SnP}^{11}$). Hence, the normal Ni–P and Ni–Sn bond distances differ by some 30 pm. Thus a favourable coordination situation for the Ni(2) atoms would be a trigonal bipyramid of composition NiP_3Sn_2 (Fig. 3). It is tempting to suggest that a preferred clustering around the Ni(2) atoms takes place with formation of NiP_3Sn_2 units (which, for the high-temperature phase or the corresponding metastable quenched room-temperature phase, do not agglomerate into larger clusters on a long-range scale).

The phase diagram data in Fig. 1 show that the NiAs-type solid solution regime tends to separate into two parts at lower temperatures. Of these, the Ni-poor part was focused on in the present PXD, PND and single-crystal X-ray diffraction study. According to the hypothesis presented above, the Ni(2) and phosphorus content may be

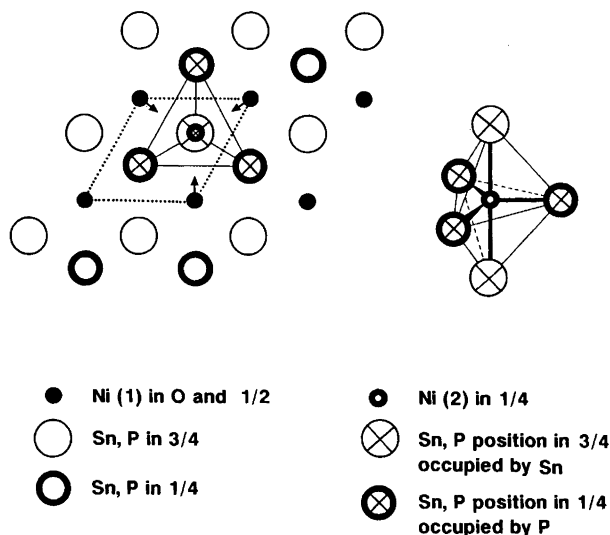


Fig. 3. Schematic drawing (right) of possible NiP_3Sn_2 cluster around Ni(2) in the trigonal bipyramidal site. Also shown (left) is the cluster as part of the structure projected on the ab -plane (z -coordinates on the figure). The tentative displacement of neighbouring Ni(1) away from ideal octahedral site is indicated with arrows.

correlated. The maximum amount of Ni(2) under these conditions is 0.15 ± 0.02 per formula unit (Figs. 1 and 2b). If all phosphorus is confined to Ni(2) P_3Sn_2 clusters, the maximum value for x is 0.45 ± 0.06 . This does indeed fit the solid solubility data presented in Fig. 1. The large thermal parameters for Ni(1) can then also be rationalized. Consider a Ni(1) X_6 ($X = \text{P}, \text{Sn}$) octahedron neighbouring a NiP_3Sn_2 unit; two of its non-metal atoms will then be P and one will be Sn, and the remaining three may for the sake of argument also be Sn atoms. In order to fulfill the bonding requirements better, the Ni(1) atom may be displaced towards the P atoms, thereby appearing in the diffraction analysis as a smeared atom. Shifts of the interstitial atoms out of their ideal trigonal bipyramidal sites have earlier been reported for e.g. Mn_{1+m}Sb ,¹⁹ and here give rise to large displacement parameters for Ni(2). EXAFS experiments are planned in order to gain more insight into the clustering processes in NiAs-type solid solutions.

Thermal expansion and physical properties. High-temperature PXD experiments were carried out for quenched and slowly cooled samples. Typically, a quenched $\text{Ni}_{1+m}\text{Sn}_{1-x}\text{P}_x$ single-phase sample, which is metastable at room temperature (cf. Fig. 1), transforms into a multiphase mixture upon heating before it enters the

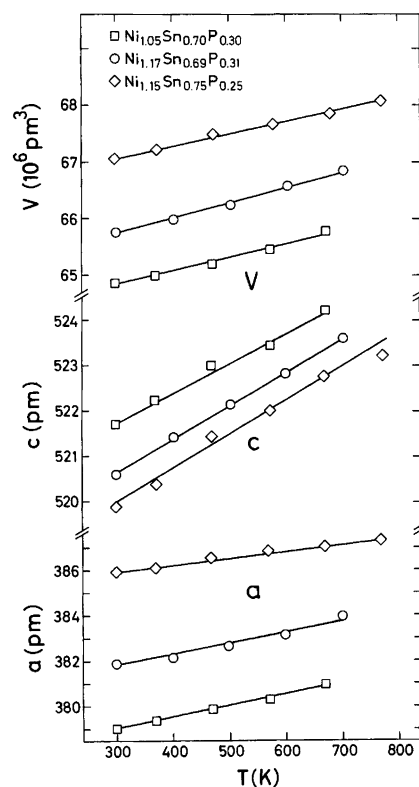


Fig. 4. Variation of unit-cell dimensions with temperature for $\text{Ni}_{1.05}\text{Sn}_{0.70}\text{P}_{0.30}$, $\text{Ni}_{1.15}\text{Sn}_{0.69}\text{P}_{0.31}$ and $\text{Ni}_{1.17}\text{Sn}_{0.75}\text{P}_{0.25}$. Calculated standard deviations do not exceed the size of the symbols.

stable regime of the NiAs-type solution phase. Only for slowly cooled samples which are inside the single-phase region in Fig. 1c is the NiAs-type phase stable over the entire interval 300–1200 K. For, e.g., quenched $\text{Ni}_{1.15}\text{Sn}_{0.75}\text{P}_{0.25}$, the metastable NiAs-type phase decomposes into $\text{Ni}_{7\pm x}\text{Sn}_8$ and Ni_2P on heating at 700 K.

The Guinier–Simon photographs yield information on the lower stability limit for the high-temperature NiAs-type phase. (Problems caused by slow kinetics should be kept in mind.) For, e.g., $\text{Ni}_{1.10}\text{Sn}_{0.93}\text{P}_{0.07}$, $\text{Ni}_{1.10}\text{Sn}_{0.84}\text{P}_{0.16}$ and $\text{Ni}_{1.15}\text{Sn}_{0.65}\text{P}_{0.35}$, the reactions of multiphased mixtures into one single NiAs-type phase occur at 830, 810 and 1070 K, respectively.

Representative temperature dependencies of the a - and c -axes are given in Fig. 4. The thermal expansion is non-linear over the interval 300–1000 K. The estimated linear thermal expansion coefficient for the unit-cell volume is $\alpha_V \approx 4.1 \times 10^{-5} \text{ K}^{-1}$ for $\text{Ni}_{1.17}\text{Sn}_{0.69}\text{P}_{0.31}$, which concurs well with corresponding values for $\text{Ni}_2\text{SnP}^{11}$ and Ni_3Sn_2 .¹⁶

The magnetic susceptibilities between 5 and 300 K for various samples of the $\text{Ni}_{1+m}\text{Sn}_{1-x}\text{P}_x$ solid solution phase indicate a weak, almost temperature-independent paramagnetism for all samples, with X_g varying between 3×10^{-6} and 5×10^{-6} e.m.u./g. These values should be corrected for diamagnetic contributions from the core electrons (about -0.2×10^{-6} e.m.u./g). In conclusion, the NiAs-type solid solution phase should be regarded as Pauli paramagnetic.

References

1. Toman, K. *Acta Crystallogr.* 4 (1951) 462.
2. Pfisterer, H. and Schubert, K. *Z. Metallk.* 41 (1950) 358.
3. Bitti, R. R., Dixmier, J. and Guinier, A. *C.R. Acad. Sci. (Paris), Ser. B* 266 (1968) 565.
4. Heyding, R. D. and Calvert, L. D. *Can. J. Chem.* 35 (1957) 449, 1205.
5. Kjekshus, A. and Walseth, K. *Acta Chem. Scand.* 23 (1969) 2621.
6. Hägg, G. and Funke, G. *Z. Phys. Chem., Teil B* 6 (1929) 272.
7. Ellner, M. J. *Less-Common Met.* 48 (1976) 21.
8. Bhargava, M. K. and Schubert, K. *J. Less-Common Met.* 33 (1973) 181.
9. Larsson, E. *Arkiv Kemi* 23 (1964) 335.
10. Brand, P. and Briest, J. *Z. Anorg. Allg. Chem.* 337 (1965) 209.
11. Furusetth, S. and Fjellvåg, H. *Acta Chem. Scand., Ser. A* 39 (1985) 537.
12. Hewat, A. W. *UKAERE Harwell Report RRL 73/897*, Harwell 1973.
13. Mallinson, P. R. and Muir, K. W. *J. Appl. Crystallogr.* 18 (1985) 51.
14. Nowotny, H. and Schubert, K. *Metallforsch.* 1 (1946) 23.
15. Brand, P. *Z. Anorg. Allg. Chem.* 353 (1967) 270.
16. Fjellvåg, H. and Kjekshus, A. *Acta Chem. Scand., Ser. A* 40 (1986) 23.
17. Furusetth, S. and Fjellvåg, H. *Acta Chem. Scand., Ser. A* 40 (1986) 695.
18. Jeitschko, W. and Jaberg, B. *Acta Crystallogr., Sect. B* 38 (1982) 598.
19. Yamaguchi, Y. and Watanabe, H. *J. Phys. Soc. Jpn.* 48 (1980) 435.

Received June 14, 1993.